Progress in Additive Manufacturing
https://doi.org/10.1007/s40964-024-00568-2

FULL RESEARCH ARTICLE

High thermal conductivity continuous pitch carbon fiber 3D printed using a 6-axis robot arm

Sinan Olcun[1] · Ahmed Elkholy[1] · Roger Kempers[1]

Received: 4 October 2023 / Accepted: 20 January 2024
© The Author(s), under exclusive licence to Springer Nature Switzerland AG 2024

Abstract

Previous research showed that continuous pitch carbon fibers (PCF) could be 3D printed and resulted in composites with moderately high effective thermal conductivities despite a relatively large degree of fiber breakage. This study presents an alternative method to 3D print continuous PCF composites using a modified fused filament fabrication extruder and a 6-axis robotic arm to understand factors affecting fiber breakage and explore the thermal performance of different printed individual raster geometries. Continuous pitch carbon fibers were coated with polylactic acid (PLA) to create PCF filaments, which were then fed into a single nozzle extruder mounted to a 6-axis robot arm for motion control. The nozzle was angled with respect to the printing surface to reduce fiber breakage during extrusion. Rasters were printed at a range of extrusion angles, and shallower angles resulted in higher effective fiber conductivity (up to 82% of the specified fiber conductivity). The ability to articulate the angled nozzle during printing was leveraged to print continuous curved raster paths and corners with different radii of curvature. These geometries were investigated to simulate potential printing practices and understand limitations of these geometries on the resultant thermal conductivity of the samples. Generally, samples printed with a radius of less than 30 mm showed a decrease in thermal conductivity and that sharp angles caused significant fiber breakage.

Keywords Pitch carbon fiber · 3D-printed composites · Continuous fibers · Thermal conductivity · Lightweight heat exchangers · Robot arm

1 Introduction

Polymer heat sinks and heat exchangers can be viable in many applications [1], especially where lightweight thermal solutions are important such as aerospace, automotive, and electronics applications [2–4]. Thermal performance can be limited by the polymer thermal conductivity [5]; however, by leveraging the additive manufacturing (AM) of polymer composites, thermal performance can be improved by both higher conductivity composite materials [6] and through the freedom to design and fabricate complex geometries for improved convection [7, 8]. For these reasons, there has been recent interest in studying AM polymer composite heat exchange technologies [9–12]; however, these composites have been exclusively discontinuous which limits their thermal conductivity [13, 14].

The shortcomings of discontinuous composites can often be improved using continuous fiber composites [15]. Historically, the continuous fibers used are typically natural, glass, and polyacrylonitrile (PAN) carbon fibers (CF) [16–19]. These fillers, (especially PAN CF) in conjunction with improved fused filament fabrication (FFF) 3D-printing techniques, have allowed for significant improvements in mechanical properties of the resulting polymer composites [20] and typically result in composites with better mechanical properties than those with discontinuous fillers [21]. Thermal conductivity, which is important for lightweight heat exchange applications, is often overlooked and most studies which investigate the thermal conductivity of FFF composites also focus on discontinuous fillers [22–24]. Notable exceptions are studies by Ibrahim et al. [25], which characterized the effective thermal conductivity of continuous PAN carbon fibers, and Ibrahim et al. [26], which developed a continuous metal wire FFF process for increased effective thermal conductivity [27].

In contrast to PAN carbon fibers (which are derived from a synthetic polymer), pitch carbon fibers (PCF) are derived

✉ Roger Kempers
kempers@yorku.ca

[1] Department of Mechanical Engineering, York University, Toronto, Canada

from petroleum or coal tar pitches and undergo a graphitization process. As PCFs can have very high thermal conductivities (up to ≈800 W/mK in the case of Mitsubishi Chemicals K13D2U), they have been employed in FFF in discontinuous form by Ji et al. to fabricate samples with thermal conductivities of 7.36 W/mK using a volume fraction of 12% PCF [28]. If PCF can be printed in a continuous form, models suggest that only 20% volume fraction is required to achieve an effective thermal conductivity of 167 W/mK which would rival the performance of many aluminum alloys used in heat exchange applications but with only half the density [25]. The printing of continuous PCF in FFF processes is challenging, however, due to the brittle nature and high tensile modulus of PCF [29, 30]. FFF extruders typically extrude at a right angle to the print bed and such a sharp bend causes the PCF to break upon exiting the nozzle.

A method for 3D printing pitch-based carbon fiber composites was developed previously and used to print multi-layer composite samples with unidirectional fibers. This approach used a print nozzle that was angled at 45° from the print bed to help mitigate breakage [31]. The resultant composites demonstrated very high stiffness [32] and thermal conductivities of up to 37.1 W/mK with a relatively low volume fraction of pitch carbon fiber (9.5%) [31]. However, in both studies, the stiffness and the effective thermal conductivity were significantly lower than theoretically predicted. Micro-computed tomography analysis showed a degree of fiber breakage had occurred resulting in discontinuities in the heat flow paths [31]. Moreover, this process was limited to printing only unidirectional samples.

An alternative to conventional FFF printers is to employ a 6-axis robot to serve as the motion control platform. A robot arm with a large working area and sufficiently high accuracy and repeatability can improve print quality through better control of fiber alignment and more complex geometries, and support the fabrication of larger components [33]. Yao et al. showed that using the greater mobility of a 6-axis robot can be leveraged to print on non-flat surfaces while avoiding staircase effects and collision resulting in parts with improved strength compared to conventional flat slicing [34]. High-performance continuous PAN carbon fiber composites have also been printed using a robot arm by Miri et al. which demonstrated high strength and stiffness [35] and Abedi et al. with good electromagnetic shielding properties [36]. The improved range of motion offered by robot arms was used by İpekçi and Ekici to 3D print continuous carbon fiber and successfully printed hollow tubes with bends and without any staircasing [37].

Here we present a new method for printing continuous PCF using a 6-axis robot arm which leverages the additional degrees of freedom to angle the print nozzle relative to the build plate such that the bending stress applied to the PCF at the nozzle exit be reduced to better mitigate fiber breakage. Moreover, this angled nozzle can be articulated to follow the raster path, allowing for curved rasters to be printed. This approach can potentially afford design flexibility for components with internal high-conductivity pathways and strategically designed thermal networks. We investigate these methods by quantifying the effective thermal conductivity of single 3D-printed PCF composite rasters to understand factors which contribute to fiber breakage. In this way, the continuous PCF 3D-printing process can be improved to result in 3D-printed composite materials with improved thermal properties more suitable for lightweight heat exchange applications.

2 Experimental methods

2.1 Materials and fiber preparation

The pitch carbon fiber investigated in the present study was manufactured by Mitsubishi Chemical Carbon Fiber and Composites with the specified properties summarized in Table 1.

Prior to 3D printing, the PCF was first coated with molten polylactic acid (PLA) pellets (3DXTECH) which was allowed to solidify to create a rigid PCF filament amenable to printing through a direct drive extrusion system. This coating was performed using a custom pultrusion setup, as shown in Fig. 1a, which included the molten PLA bath through which the PCF was passed. After the polymer bath, the PCF was pulled through an 0.8-mm nozzle and allowed to cool at room temperature and solidify. Expansion after the nozzle resulted in a continuous PCF filament approximately 1 mm in diameter and the resulting volume percentage of this filament was approximately 24% PCF as shown in Fig. 1b (estimated using the specified fiber count and fiber diameter from Table 1).

Table 1 Pitch carbon fiber properties [38]

Pitch carbon fiber	Tow fiber count	Fiber diameter (μm)	Tensile modulus (GPa)	Tensile strength (MPa)	Density (g/cm^3)	Thermal conductivity (W/mK)
K13D2U (D2U)	2000	11	935	3700	2.20	800

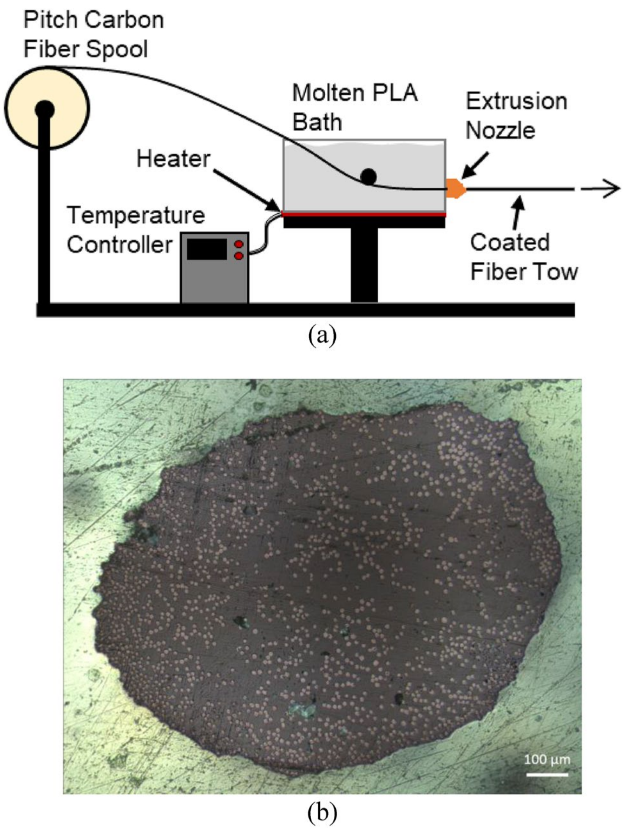

Fig. 1 **a** Coating pitch carbon fiber tows with PLA, **b** cross-section of PLA-coated PCF

2.2 Continuous fiber printer extruder and movement control

In the two previous investigations which 3D printed continuous pitch carbon fiber, the 3D printer used a fixed angle hot end which resulted in the PCF extruding at a constant 45° relative to the print bed [31, 32]. The fixed angle limited the printer to only printing unidirectional samples along the *x*-axis, severely limiting the complexity of printed parts. To overcome these limitations, a new extruder was designed and fitted on a 6-axis robot arm, which allows the nozzle to be angled in any direction and for full articulation of the nozzle during printing. In this way, the angled nozzle can be articulated to follow the path of a curved raster.

The extruder design is shown in Fig. 2a. It consists of a V6 hot end (E3D-Online) with a custom nozzle which was machined to be longer and slenderer such that the entire extruder could be angled to a large degree without hitting the printing surface (Fig. 2a).

An all-metal V6 extruder (E3D-Online) served as basis for this extruder and uses the original heatsink, hot-end, heat-break, heater, and thermistor. However, the nozzle was custom machined to be longer and slenderer than the stock nozzle and allows for the whole extruder to be angled up to 65° from vertical without hitting the printing surface (illustrated in Fig. 2b). To decrease friction between the filament and extruder walls, the internal walls of the extruder and nozzle were coated with a polytetrafluoroethylene (PTFE) spray (Synco Chemical).

The extruder was mounted on an ABB IRB 1200 7–0.7 6-axis arm as shown in Fig. 2b and the arm and a heated print bed were mounted to a steel table. The print bed was coated with a 0.15 mm polyethylenimine (PEI) sheet (Spool3D) to promote raster adhesion, and bed leveling was performed using four compression springs adjusted with screws at the corners of the print bed.

The robot arm motion was controlled via an IRC5 compact controller, and the extruder was controlled with a RAMPS 1.4 control board. G-code was prepared and ran simultaneously on the two controllers to print samples. For the straight samples, the G-code was written by hand. For the curved samples, the open-source tool FullControl GCode Designer was used (Loughborough University) to generate the G-code. The G-code was then converted to motion in the robot arm using RobotStudio 3D Printing PowerPac (ABB).

For this study, the single raster samples were 3D printed at a speed of 13.3 mm/s, hot end temperature of 220 °C, and a bed temperature of 60 °C.

2.3 Fiber and raster thermal conductivity measurement apparatus

The steady-state fiber conductivity approach developed in the present study is shown in Fig. 3a and is akin to setups developed by Piraux et al. [39] and May et al. [40].

The sample under test is clamped between a heater, which applies a known input power to the sample, and a cooling block which holds the other end of the sample at fixed temperature as shown in Fig. 3a. Temperature sensors placed along the sample measure the temperature gradient and at steady state, the thermal resistance of the sample can be computed.

The heater consists of small copper clamp with an embedded thermistor (GAG22K7MCD419, TE Connectivity) which served as a heating element. Electrical power (Q_{input}) to the heater was supplied and measured using a Keithley 2400 SourceMeter. The other end of the sample was clamped to a copper cooling block which was temperature controlled using a PID controlled thermoelectric water chiller. The resulting temperature gradient along the sample was then measured using two carefully calibrated thermistors placed in contact with the samples at a known spacing, *L*. The two sensing thermistors were measured using a Lakeshore Model 370 AC Resistance Bridge to accurately measure their resistance with minimal self-heating using a four-wire configuration. The thermistors were calibrated together against a reference probe (5606 Full Immersion PRT, Fluke) in a

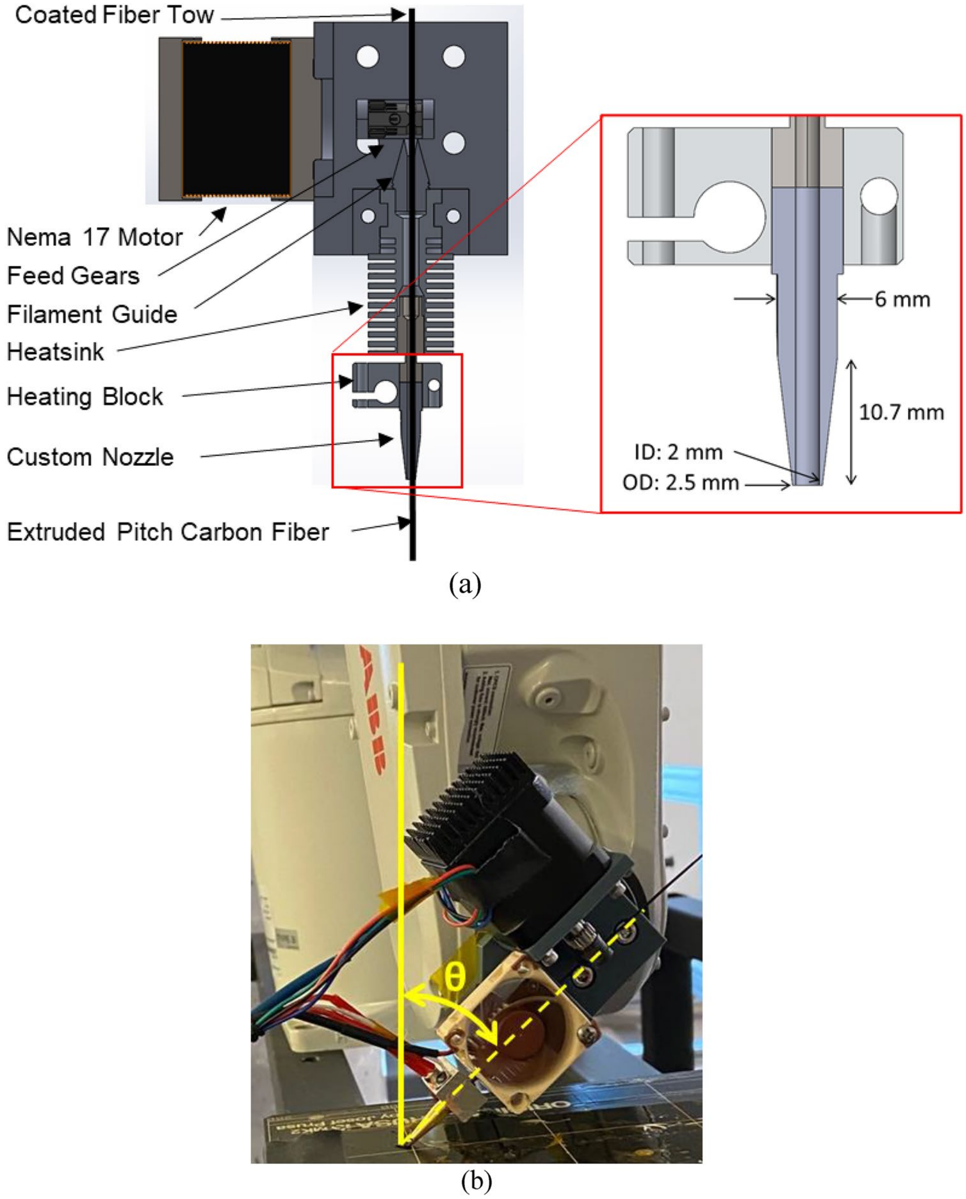

Fig. 2 **a** Schematic of the continuous PCF extruder nozzle including detailed view of nozzle, **b** photograph of the extruder mounted to the robot arm illustration nozzle articulation

uniform temperature environment like that described in Ref. [41], such that the resistors were found to show the same temperature reading with a maximum uncertainty of approximately ± 0.02 K.

The thermal resistance of the sample is quantified as

$$R_{\text{sample}} = \frac{T_1 - T_2}{Q_{\text{sample}}} \tag{1}$$

where T_1 and T_2 are the measured temperatures across the sample and Q_{sample} is the heat transfer rate through the sample quantified using the electrical input power less any heat loss to the ambient (described below). The effective thermal conductivity of the fibers in the sample was then calculated as

$$k_f = \frac{L}{\left(R_{\text{sample}}\right)A_f} \tag{2}$$

where L is the distance between the temperature measurements measured using calipers (with an estimated uncertainty of 1 mm), and A_f is the cross-sectional area of the conductive fibers calculated from the specified diameter of the fibers and the fiber count per tow (this assumes that all heat flow through the sample is conducted through fibers and not the polymer).

This method relies on the assumption that all input power to the heater flows through sample and therefore minimal heat loss to the ambient. This was achieved by placing the whole test section under vacuum to minimize heat transfer through the ambient air like Refs. [39] and [40]. The bell

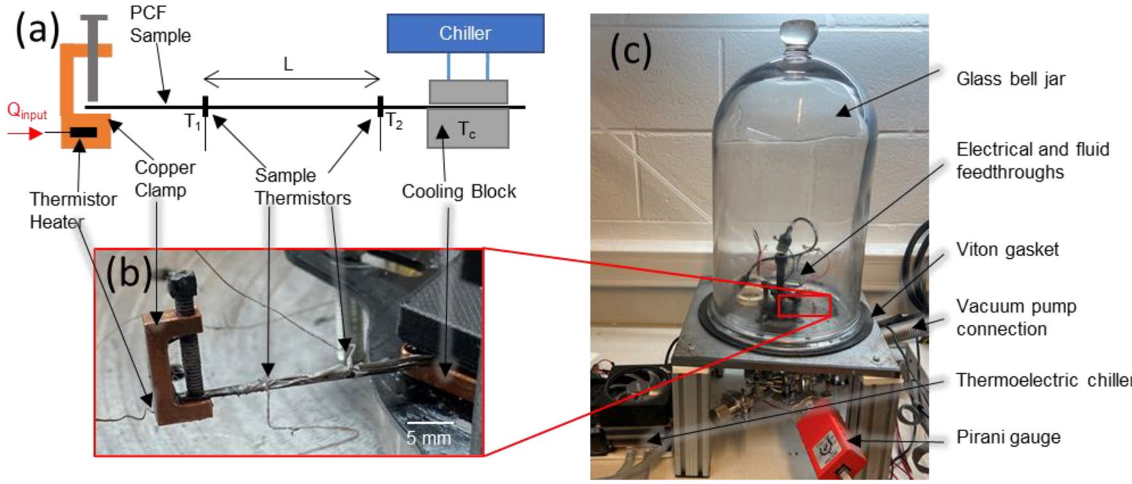

Fig. 3 Apparatus for measuring the thermal conductivity of 3D-printed continuous fiber rasters **a** schematic of approach, **b** close-up photograph of sample test section, **c** photograph of experimental setup

jar setup shown in Fig. 3c was used to enclose the sample test section. Electrical and fluid feedthroughs were used to connect the thermistor wires and to temperature control the cooling block. Vacuum was achieved using a rotary vane pump (Edwards V5) which is specified for 10^{-3} mbar. A Pirani gauge (EDWARDS APG-L-NW16) was used to measure the vacuum within the chamber. Outgassing was minimized by thoroughly cleaning and heating the inner surfaces of the chamber to remove any contaminants. Sample thermal measurements were only considered once the chamber pressure reached 2×10^{-3} mbar to lower the thermal conductivity of air to 4% of its nominal value at atmospheric pressure [42] and obtain sufficiently accurate measurements of k_f using this technique.

During measurements, the cold block was held at ≈14 °C and the hot clamp was supplied with approximately 40 mW. The ambient temperature in the chamber was kept at 22 °C. The distance between thermistors T_1 and T_2 on the samples was approximately 20 mm for each sample such that a sufficiently large temperature difference could be measured with good accuracy (typically 3 to 5 K depending on thermal conductivity of the sample for input powers of on the order of $\approx 10^{-2}$ W). Temperature and input power measurements were collected and displayed by a MATLAB script. All tests were run until steady state was achieved.

2.4 Uncertainty analysis and heat loss calibration

A summary of the measured quantities, their measurement technique, and their associated uncertainties is presented in Table 2.

The uncertainty of k_f was quantified using the individual measurement uncertainties and the error propagation method described by Kline and McClintock [43]. The uncertainty of the calculated quantity, U_Z, is expressed generally as

$$U_Z = \sqrt{\sum_{i=1}^{n} \left[\frac{\partial Z}{dx_i} U_i \right]^2} \tag{3}$$

where Z is the calculated quantity expressed in terms of the measured quantities, x_i, having the uncertainties U_i. The resultant uncertainty in k_f was approximately 8%.

The vacuum bell jar does not eliminate all heat loss during sample testing and a heat loss calibration was performed to account for the small heat leakage from the heater clamp to the ambient environment by suspending the clamp within the evacuated bell jar and inputting relatively small input powers to the heater thermistor. A relationship between the steady-state heat transfer rate and the temperature difference between the clamp and ambient temperature was established

Table 2 Measured parameters and uncertainties

Measured parameter	Instrument or source of uncertainty	Uncertainty
Voltage, V	Keithley 2400 SourceMeter	±0.02%
Current, I	Keithley 2400 SourceMeter	±0.02%
Sample length, L	Digital Caliper	±1 mm
Fiber diameter, d_f	Naito et al. [29]	±0.5 µm
Temperature difference, ΔT	Lakeshore 370 AC Resistance Bridge	±0.02 K

to account for this loss and provide a better estimate of Q_{sample} used in Eq. 1.

3 Results and discussion

3.1 Baseline thermal conductivity measurements

The accuracy of the thermal conductivity apparatus was verified by measuring the thermal conductivities of different metal wires with known thermal conductivities over a range of input powers. Figure 4 shows the measured thermal conductivities of a 28 AWG Copper 110 wire, an 18 AWG Aluminum 1100 wire, and a 1.5 mm diameter 99% tin solder wire as a function of heater input power. The average measured thermal conductivity of the aluminum and tin samples was 214.7 W/mK and 64.8 W/mK, respectively, which agrees well with the accepted values of 220 W/mK and 66 W/mK, respectively, the measured values being only 2.45% and 1.9% away from the accepted values. For the coper wire sample, the average measured thermal conductivity was 409.8 W/mK which is about 5% higher than the accepted value 390 W/mK. Uncertainty propagation led to high uncertainties for the copper wire sample, which stemmed from its relatively small wire diameter (the aluminum and tin wire samples had lower uncertainty due to larger diameters).

3.2 Effect of extruder angle

The effective fiber thermal conductivity was measured for individual straight rasters printed using nozzles angled from 45° to 60° from normal (see Fig. 2b) and the results are plotted in Fig. 5. All samples were printed using the

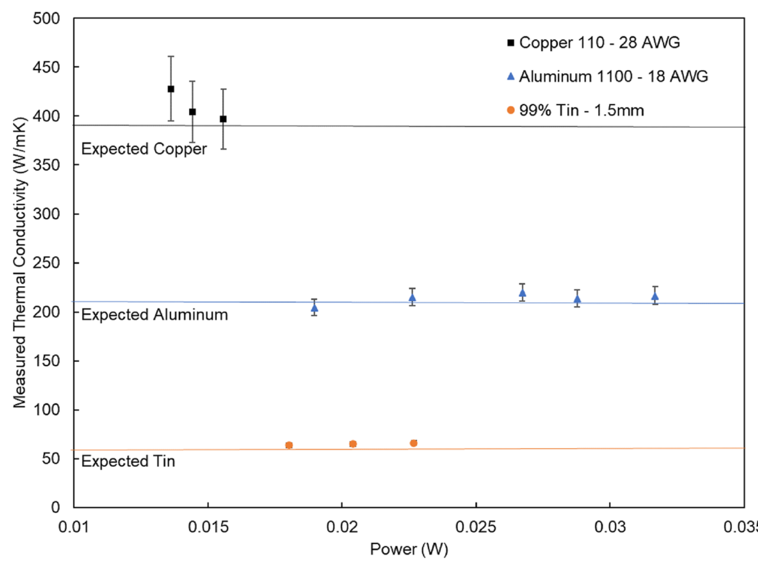

Fig. 4 Measured thermal conductivity of different wires at different input power values

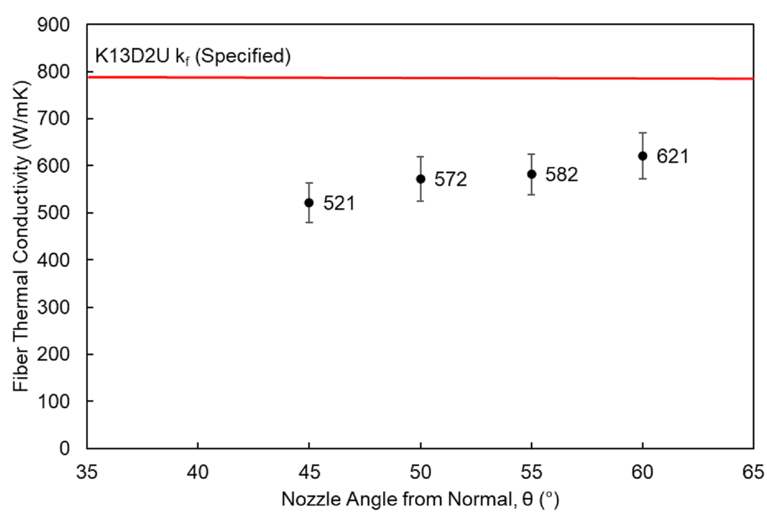

Fig. 5 Measured thermal conductivity of PCF rasters printed at varying nozzle angles

same parameters and g-code settings, except for print angle which was varied in 5° intervals from 45° to 60°. At 45°, the measured k_f was 521 W/mK but this increased with nozzle angle achieving 621 W/mK when the extruder was oriented at 60° from vertical. This suggests that that shallower print angles between the heated bed and nozzle result in less PCF breakage during printing; this results in higher thermal conductivities that are much closer to those of the original unprocessed fiber with the 60° sample having a k_f of 82% of specified K13D2U thermal conductivity.

3.3 Effect of curvature radius

The previous section demonstrated that shallower nozzle angles resulted in increased effective thermal conductivity of the printed composite; however, to fully leverage the benefits of continuous PCF for thermal applications, the ability to design and control the directionality of the conductive fibers is essential for many applications. To assess these effects, curved continuous PCF rasters were printed with the nozzle held at a constant 55° from vertical and articulating to stay tangent to the curve during printing to evaluate the effect of curvature radius on the effective thermal conductivity of the printed raster. This angle was used because it achieved a reasonably k_f and allowed for consistent sample adhesion to the print bed. Samples with a range radius of curvature were printed as shown in Fig. 6a, and the resultant effective thermal conductivity of these fibers, k_f, is plotted in Fig. 6b. Samples printed with a radius between 30 and 50 mm had thermal conductivities nominally the same (within measured uncertainty) as the previously measured linear raster printed at 55° of 582 W/mK. The sample printed at a radius of 20 mm was then shown to decrease thermal conductivity and at a radius of 15 mm, the lowest thermal conductivity of 376 W/mK was measured (or 53% less than the original K13D2U fiber thermal conductivity).

3.4 Effect of cornering technique

The ability to print corners is also important for more complex 3D-printed parts; hence, samples which underwent local changes in direction were also printed. Like the previous section, the PCF rasters were printed with the nozzle held at a constant 55° from vertical. The samples were then printed with a straight approach section, followed by a corner creation process, and then a straight exit path. The turning point process involved the nozzle instantaneously turning to create a corner with varying angles (150°, 120°, 90°) as shown in Fig. 7a (i.e., with an r_c of ≈0). It was found that sharp corners printed by turning the nozzle instantaneously at the corner yielded additional breakage, as evidenced by the markedly lower thermal conductivity measured in these samples (Fig. 7b). For a corner with an angle of 120°, a fiber thermal conductivity of 345 W/mK was measured (43% of the original thermal conductivity of K13D2U) while corners at 90° had full breakage.

Although sharp corners performed relatively poorly (especially at smaller angles), the use of a constant radius of curvature instead of a sharp corner achieved the same general shape and change in printing direction as shown in Fig. 7c. Incorporating a radius of curvature, r_c of 20 mm at the corners yielded thermal conductivities consistent with the continuous $r_c = 20$ mm case from Fig. 5, for all turning angles, as shown in Fig. 7d.

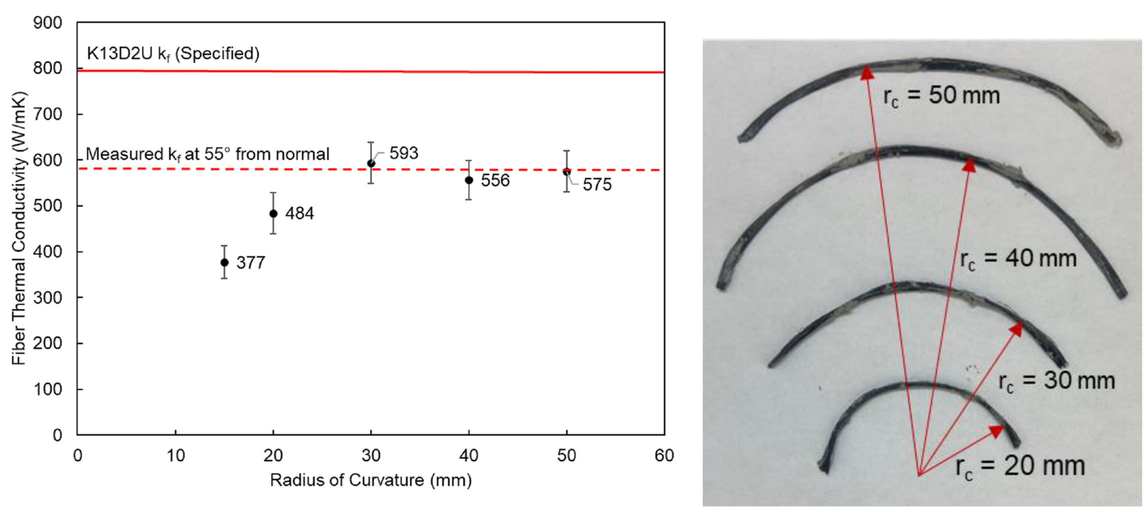

(a) (b)

Fig. 6 **a** Measured fiber thermal conductivities as a function of printed of radii of curvature, r_c, **b** representative images of samples prior to cutting for thermal testing ($r_c = 15$ mm sample not shown)

Fig. 7 **a** Corner samples printed using a turn point method, **b** corresponding fiber thermal conductivities, **c** corner samples printed using a constant turning radius, **d** corresponding fiber thermal conductivities

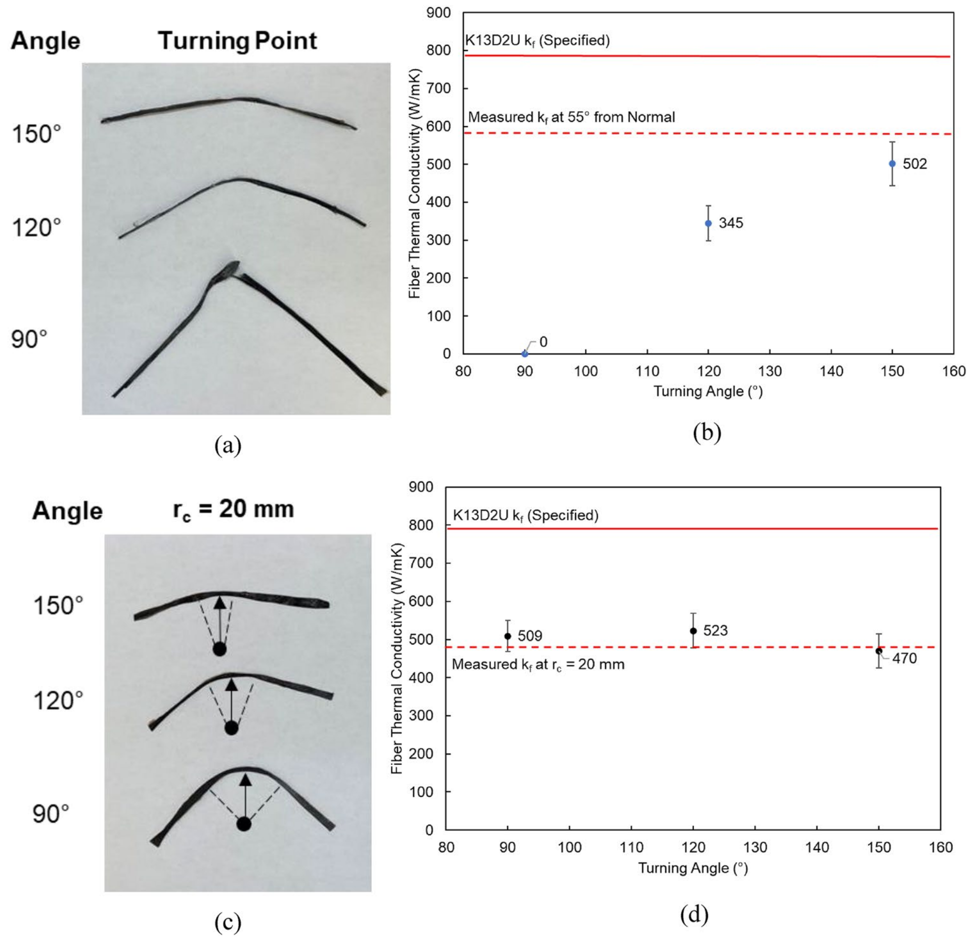

4 Summary and outlook

A method for fabricating high-conductivity continuous pitch carbon fiber composites using 6-axis robot arm FFF 3D printing is presented. Continuous pitch carbon fibers were coated in a PLA before being printed using a custom extruder mounted to a 6-axis robot arm. The robot arm was used to angle the printer nozzle with respect to the print bed to decrease the amount of continuous fiber breakage and increase the effective thermal conductivity of the printed rasters. The robot arm further allowed for the nozzle to be angled and articulated in the direction of printing, thereby affording more complex continuous fiber raster paths. Continuous curves with a range of curvature radii were investigated; radii of curvatures of less than 30 mm should be avoided to maintain fiber thermal conductivity. Moreover, approaches to creating corners within raster traces were investigated and showed that sharp corners with low radii of curvature should also be avoided.

Future research should address improvement of the nozzle design itself to further mitigate fiber breakage and understand impacts on raster adhesion. Microscopic imaging to understand the precise mechanism of fiber breakage may also be useful.

This understanding can help support the fabrication of larger-scale continuous PCF composites with controllable anisotropic heat flow paths. It will further support the design of functional thermal composites for lightweight heat exchange applications in the automotive, aerospace, and electronics cooling sectors.

Acknowledgements The authors acknowledge the support of the Natural Sciences and Engineering Research Council of Canada (NSERC).

Funding This study was supported by Natural Sciences and Engineering Research Council of Canada, Grant No. RGPIN-2018-05879.

Data availability Data will be made available on request.

Declarations

Conflict of interest On behalf of all authors, the corresponding author states that there is no conflict of interest.

References

1. Mikulionok IO (2019) Use of polymer materials in heat exchangers (review of patents). Chem Pet Eng 55:687–695. https://doi.org/10.1007/s10556-019-00680-z
2. Narumanchi S, Mihalic M, Moreno G, Bennion K (2012) Design of light-weight, single-phase liquid-cooled heat exchanger for automotive power electronics. In: 13th InterSociety conference on thermal and thermomechanical phenomena in electronic systems, pp 693–699. https://doi.org/10.1109/ITHERM.2012.6231495.
3. Liu Q, Xu G, Wen J, Fu Y, Zhuang L, Dong B (2022) Multivariate design and analysis of aircraft heat exchanger under multiple working conditions within flight envelope. ASME J Therm Sci Eng Appl 14(6):061003. https://doi.org/10.1115/1.4052342
4. Samudre P, Kailas SV (2022) Thermal performance enhancement in open-pore metal foam and foam-fin heat sinks for electronics cooling. Appl Therm Eng 205:117885. https://doi.org/10.1016/j.applthermaleng.2021.117885
5. Hussain ARJ et al (2017) Review of polymers for heat exchanger applications: factors concerning thermal conductivity. Appl Therm Eng 113:1118–1127. https://doi.org/10.1016/j.applthermaleng.2016.11.041
6. Vadivelu MA, Ramesh Kumar C, Joshi GM (2016) Polymer composites for thermal management: a review. Compos Interfaces. https://doi.org/10.1080/09276440.2016.1176853
7. Moon H, Boyina K, Miljkovic N, King WP (2021) Heat transfer enhancement of single-phase internal flows using shape optimization and additively manufactured flow structures. Int J Heat Mass Transf 177:121510. https://doi.org/10.1016/j.ijheatmasstransfer.2021.121510
8. Unger S, Beyer M, Pietruske H, Szalinski L, Hampel U (2021) Air-side heat transfer and flow characteristics of additively manufactured finned tubes in staggered arrangement. Int J Therm Sci 161:106752. https://doi.org/10.1016/j.ijthermalsci.2020.106752
9. Timbs K, Khatamifar M, Antunes E, Lin W (2021) Experimental study on the heat dissipation performance of straight and oblique fin heat sinks made of thermal conductive composite polymers. Therm Sci Eng Prog 22:100848. https://doi.org/10.1016/j.tsep.2021.100848
10. Ahmadi B, Bigham S (2022) Performance evaluation of hi-k lung-inspired 3D-printed polymer heat exchangers. Appl Therm Eng 204:117993. https://doi.org/10.1016/j.applthermaleng.2021.117993
11. Arie MA, Hymas DM, Singer F, Shooshtari AH, Ohadi M (2020) An additively manufactured novel polymer composite heat exchanger for dry cooling applications. Int J Heat Mass Transf 147:118889. https://doi.org/10.1016/j.ijheatmasstransfer.2019.118889
12. Deisenroth DC, Moradi R, Shooshtari AH, Singer F, Bar-Cohen A, Ohadi M (2018) Review of heat exchangers enabled by polymer and polymer composite additive manufacturing. Heat Transf Eng 39(19):1648–1664. https://doi.org/10.1080/01457632.2017.1384280
13. Qin Y et al (2016) Interfacial interaction enhancement by shear-induced β-cylindrite in isotactic polypropylene/glass fiber composites. Polymer 100:111–118
14. Yu K, Wang M, Wu J, Qian K, Sun J, Lu X (2016) Modification of the interfacial interaction between carbon fiber and epoxy with carbon hybrid materials. Nanomaterials 6(12):89
15. Liu G, Xiong Y, Zhou L (2021) Additive manufacturing of continuous fiber reinforced polymer composites: design opportunities and novel applications. Compos Commun 27:100907. https://doi.org/10.1016/j.coco.2021.100907
16. Kabir SMF, Mathur K, Seyam A-FM (2020) A critical review on 3D printed continuous fiber-reinforced composites: history, mechanism, materials and properties. Compos Struct 232:111476. https://doi.org/10.1016/j.compstruct.2019.111476
17. Omar NWY, Shuaib NA, Hadi MHJA, Azmi AI (2019) Mechanical properties of carbon and glass fibre reinforced composites produced by additive manufacturing: a short review. IOP Conf Ser Mater Sci Eng. https://doi.org/10.1088/1757-899X/670/1/012020
18. Valvez S, Santos P, Parente JM, Silva MP, Reis PNB (2020) 3D printed continuous carbon fiber reinforced PLA composites: a short review. Procedia Struct Integr 25:394–399. https://doi.org/10.1016/j.prostr.2020.04.056
19. Dickson AN, Abourayana HM, Dowling DP (2020) 3D printing of fibre-reinforced thermoplastic composites using fused filament fabrication—a review. Polymers. https://doi.org/10.3390/POLYM12102188
20. Çevik Ü, Kam M (2020) A review study on mechanical properties of obtained products by FDM method and metal/polymer composite filament production. J Nanomater. https://doi.org/10.1155/2020/6187149
21. Zhang H et al (2022) 3D printing of continuous carbon fibre reinforced powder-based epoxy composites. Compos Commun. https://doi.org/10.1016/j.coco.2022.101239
22. Brillon A et al (2022) Anisotropic thermal conductivity and enhanced hardness of copper matrix composite reinforced with carbonized polydopamine. Compos Commun 33:101210. https://doi.org/10.1016/j.coco.2022.101210
23. Elkholy A, Rouby M, Kempers R (2019) Characterization of the anisotropic thermal conductivity of additively manufactured components by fused filament fabrication. Prog Addit Manuf 4(4):497–515. https://doi.org/10.1007/s40964-019-00098-2
24. Elkholy A, Kempers R (2022) An accurate steady-state approach for characterizing the thermal conductivity of additively manufactured polymer composites. Case Stud Therm Eng 31:101829. https://doi.org/10.1016/j.csite.2022.101829
25. Ibrahim Y, Elkholy A, Schofield JS, Melenka GW, Kempers R (2020) Effective thermal conductivity of 3D-printed continuous fiber polymer composites. Adv Manuf Polym Compos Sci 6(1):17–28. https://doi.org/10.1080/20550340.2019.1710023
26. Ibrahim Y, Melenka GW, Kempers R (2018) Additive manufacturing of continuous wire polymer composites. Manuf Lett 16:49–51. https://doi.org/10.1016/j.mfglet.2018.04.001
27. Ibrahim Y, Kempers R (2022) Effective thermal conductivity of 3D-printed continuous wire polymer composites. Prog Addit Manuf. https://doi.org/10.1007/s40964-021-00256-5
28. Ji J et al (2020) Enhanced thermal conductivity of alumina and carbon fibre filled composites by 3-D printing. Thermochim Acta. https://doi.org/10.1016/j.tca.2020.178649
29. Naito K, Tanaka Y, Yang JM, Kagawa Y (2009) Flexural properties of PAN- and pitch-based carbon fibers. J Am Ceram Soc 92(1):186–192. https://doi.org/10.1111/j.1551-2916.2008.02868.x
30. Huson MG (2017) High-performance pitch-based carbon fibers. Structure and properties of high-performance fibers. Elsevier, pp 31–78. https://doi.org/10.1016/B978-0-08-100550-7.00003-6
31. Olcun S, Ibrahim Y, Isaacs C, Karam M, Elkholy A, Kempers R (2023) Thermal conductivity of 3D-printed continuous pitch carbon fiber composites. Addit Manuf Lett 4:100106. https://doi.org/10.1016/j.addlet.2022.100106
32. Saleh M, Olcun S, Karam M, Kempers R, Melenka GW (2024) High stiffness 3D-printed continuous pitch carbon fiber reinforced polymer composites. Submitted to J Compos Mater (under review)
33. Urhal P, Weightman A, Diver C, Bartolo P (2019) Robot assisted additive manufacturing: a review. Robot Comput Integr Manuf 59:335–345. https://doi.org/10.1016/j.rcim.2019.05.005
34. Yao Y, Zhang Y, Aburaia M, Lackner M (2021) 3d printing of objects with continuous spatial paths by a multi-axis robotic FFF platform. Appl Sci. https://doi.org/10.3390/app11114825

35. Miri S, Kalman J, Canart JP et al (2022) Tensile and thermal properties of low-melt poly aryl ether ketone reinforced with continuous carbon fiber manufactured by robotic 3D printing. Int J Adv Manuf Technol 122:1041–1053. https://doi.org/10.1007/s00170-022-09983-7
36. Abedi K, Miri S, Gregorash L, Fayazbakhsh K (2022) Evaluation of electromagnetic shielding properties of high-performance continuous carbon fiber composites fabricated by robotic 3D printing. Addit Manuf 54:102733. https://doi.org/10.1016/j.addma.2022.102733
37. İpekçi A, Ekici B (2021) Experimental and statistical analysis of robotic 3D printing process parameters for continuous fiber reinforced composites. J Compos Mater. https://doi.org/10.1177/0021998321996425
38. Mitsubishi Chemical Carbon Fiber and Composites, Inc (2021) Pitch fiber/ accessed 2021–11–11 (http://mccfc.com/pitch-fiber/)
39. Piraux L, Issi JP, Coopmans P (1987) Apparatus for thermal conductivity measurements on thin fibres. Measurement 5(1):2–5. https://doi.org/10.1016/0263-2241(87)90020-0
40. May PW, Portman R, Rosser KN (2005) Thermal conductivity of CVD diamond fibres and diamond fibre-reinforced epoxy composites. Diam Relat Mater 14(3–7):598–603. https://doi.org/10.1016/j.diamond.2004.10.039
41. Kempers R, Kolodner P, Lyons A, Robinson AJ (2009) A high-precision apparatus for the characterization of thermal interface materials. Rev Sci Instrum 80:0911. https://doi.org/10.1063/1.3193715
42. Manglik R. Heat transfer and fluid flow data books. Genium Publishing Corporation [Online]. Available: https://app.knovel.com/hotlink/toc/id:kpHTFFDB0F/heat-transfer-fluid-flow/heat-transfer-fluid-flow
43. Kline SJ, McClintock FA (1953) Describing uncertainties in single sample experiments. Mech Eng 75:3–8

Publisher's Note Springer Nature remains neutral with regard to jurisdictional claims in published maps and institutional affiliations.

Springer Nature or its licensor (e.g. a society or other partner) holds exclusive rights to this article under a publishing agreement with the author(s) or other rightsholder(s); author self-archiving of the accepted manuscript version of this article is solely governed by the terms of such publishing agreement and applicable law.